Available online at www.sciencedirect.com
ScienceDirect
Trans. Nonferrous Met. Soc. China 32(2022) 3860−3872
Transactions of Nonferrous Metals Society of China
www.tnmsc.cn

Effects of Cu content on microstructures and compressive mechanical properties of CNTs/Al−Cu composites

Si-wei LUO[1], Yue WU[1], Biao CHEN[2], Min SONG[3], Jian-hong YI[4], Bai-song GUO[1,5], Qi-wei WANG[1], Yong YANG[5], Wei LI[1], Zhen-tao YU[1]

1. Institute of Advanced Wear & Corrosion Resistant and Functional Materials, Jinan University, Guangzhou 510632, China;
2. State Key Laboratory of Solidification Processing, Northwestern Polytechnical University, Xi'an 710072, China;
3. State Key Laboratory of Powder Metallurgy, Central South University, Changsha 410083, China;
4. School of Materials Science and Engineering, Kunming University of Science and Technology, Kunming 650093, China;
5. Department of Materials Science and Engineering, City University of Hong Kong, Hong Kong 999077, China

Received 30 September 2021; accepted 27 December 2021

Abstract: The carbon nanotubes (CNTs) reinforced Al−Cu matrix composites were prepared by hot pressing sintering and hot rolling, and the effects of Cu content on the interfacial reaction between Al and CNTs, the precipitation behavior of Cu-containing precipitates, and the resultant mechanical properties of the composites were systematically investigated. The results showed that the increase of Cu content can not only increase the number and size of Cu-containing precipitate generated during the composite fabrication processes, but also promote the interfacial reaction between CNTs and Al matrix, leading to the intensified conversion of CNTs into Al_4C_3. As a result, the composite containing 1 wt.% Cu possesses the highest strength, elastic modulus and hardness among all composites, due to the maintenance of the original structure of CNTs. Moreover, the increase of Cu content can change the dominant strengthening mechanisms for the enhanced strength of the fabricated composites.

Key words: Al matrix composites; Al−Cu precipitates; carbon nanotubes; interfacial reaction; strengthening mechanism

1 Introduction

The demand for metal matrix composites with good comprehensive mechanical properties and lightweight is ever-increasing, due to the rapid development of advanced industries [1]. Among these, aluminum (Al) matrix composites have drawn much more attention from material researchers and engineers due to their low density, excellent deformation ability, high thermal shock resistance, high elastic modulus, high fatigue strength, and desired creep and wear resistance [2]. In particular, carbon nanotubes (CNTs) reinforced Al matrix composites (CNTs/Al) have been regarded as the promising structural composites because CNTs exhibit excellent strength (~110 GPa), ultra-high elastic modulus (~1 TPa), large aspect ratio (>1000), low density (2.1 g/cm^3) and low coefficient of thermal expansion (~0) [3], which are more effective in achieving high mechanical properties of the fabricated composites than the traditional ceramic particles.

However, although lots of effective approaches have been developed to ameliorate the dispersion state of CNTs in the Al matrix and strengthen the

Corresponding author: Bai-song GUO, Tel: +86-15700796463, E-mail: guobaisong@jnu.edu.cn;
Qi-wei WANG, Tel: +86-13929565955, E-mail: wangqiwei@jnu.edu.cn
DOI: 10.1016/S1003-6326(22)66063-1

Al−CNTs interfacial bonding. The reported strength of CNTs/Al composites is generally below 450 MPa [4]. The limited strength of CNTs/Al composites can be mostly attributed to the fact that pure Al rather than Al alloy was primarily used as the matrix [5], due to its simple system and ease of analysis. To the best of our knowledge, in comparison to pure Al matrix, taking Al alloy as the matrix can produce precipitates during the composite fabrication processes, which can play a synergic strengthening role with CNTs to improve the mechanical properties of the obtained CNTs/Al composites [6,7]. The synergic strengthening effects of the precipitates in the Al alloy matrix have also been demonstrated by SHIN and BAE [8]. According to their research, compared to the graphene reinforced pure Al matrix composite, using 2024 Al alloy as the matrix can improve the tensile strength of the fabricated composite to around 280 MPa. This previous study reveals that the Al alloy matrix is superior to the pure Al matrix in achieving higher strength of CNTs/Al composites. Thus, it is valuable to systematically investigate the microstructures and resultant mechanical properties of CNTs reinforced Al alloy matrix composites, especially for the application of high-strength Al alloy (AA2xxx and AA7xxx) as the matrix.

Unlike the CNTs reinforced pure Al matrix composite, the CNTs/Al−Cu system is much more complex due to the existence of the Cu element. With alloying with the Al matrix, the microstructure evolution during the composite fabrication process will be complicated. In other words, the original structure of CNTs is easier to be destroyed in CNTs/Al−Cu composites due to the in-situ interfacial reaction. Hence, to fully exploit the synergic strengthening effects of CNTs and precipitates for much better mechanical properties, it is necessary to investigate the unclear characteristics of microstructures and mechanical properties of CNTs/Al−Cu composites, such as the effects of the Cu content on the Al_4C_3 formation, Al−Cu precipitation and mechanical properties of such composites.

In this work, we systematically investigated the effects of Cu content on the interfacial reaction of Al matrix and CNTs, the precipitation behavior of the Cu-containing precipitates, and the resultant mechanical properties of the CNTs/Al−Cu composites. The fundamental relationship between the microstructure characteristics and mechanical properties was deeply examined. The present findings can guide the matrix composition design of CNTs reinforced Al alloy matrix composites for better mechanical properties.

2 Experimental

2.1 Fabrication of composites

The Al−Cu alloy powders were fabricated from the gas atomized pure Al powders and pure Cu powders using the mechanical alloying method. The ball/powder mass ratio, ball milling time, and rotation speed were 8:1, 5 h, and 300 r/min, respectively. To reduce the agglomeration of CNTs and promote the dispersion of CNTs in Al powders, the CNTs supplied by Sigma-Aldrich Co., Ltd. were oxidized with the same oxidization method as that in our previous study [9]. Subsequently, the synthesized Al−Cu alloy powders were added to the suspension of oxidized CNTs and ball-milled for 3 h with a ball/powder mass ratio of 5:1 and a rotation speed of 300 r/min, and a 0.5 wt.% zinc stearate was used as a process control agent. The resulting mixed suspension was thoroughly dried in a vacuum oven at 60 °C after vacuum filtration. The dried powders were further dry ball milled with the same ball-milling parameters as those in the previous solution-assisted mixing process, which can not only eliminate the possible CNTs clusters on the surface of flaky Al−Cu powders, but also promote the embedding of CNTs into the Al−Cu powders. The mixed powders were sintered at 600 °C for 30 min with a heating rate of 10 °C/min in a quick hot pressing sintering furnace (HFAS−0304D). Mechanical pressure of 40 MPa was applied to the samples throughout the sintering process. The mass of each sintered specimen is about 46 g, and the diameter and height are 40 mm and 8 mm, respectively. To further densify the sintered composites, these samples were hot-rolled with the same processes and parameters as elsewhere [10]. Three batches of composites with the same CNTs content (0.75 vol.%) and different Cu contents (1, 3, and 7 wt.%) were fabricated and denoted as Al−1Cu@CNTs, Al−3Cu@CNTs, and Al−7Cu@CNTs, respectively. The detailed fabrication processes for the desired composites are illustrated in Fig. 1.

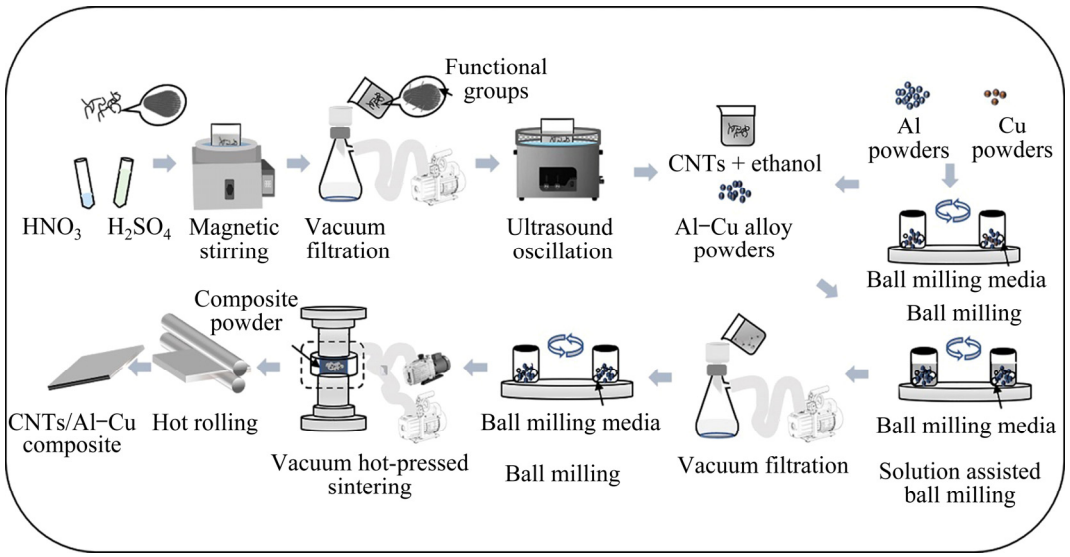

Fig. 1 Schematic diagram of preparation process of Al−Cu@CNTs composites

2.2 Characterization

FEI Nova Nano230 and Phenom XL scanning electron microscopes (SEM) and JEOL−2100F transmission electron microscope (TEM) were used to examine the microstructures of the starting powders (Al, Cu, CNTs), mixed powders, and the fabricated bulk composites. The number and average size of the precipitates were statistically analyzed based on the obtained SEM images using ImageJ analysis software. The phase compositions of the powder mixture and the prepared composites were identified by X-ray diffraction (XRD, Ultima IV) using a Cu K_α radiation source with a scanning rate of 5 (°)/min. The measured bulk density of the three composites was measured by an MI−120 MITR metal density tester (the density resolution: 0.001 g/cm^3) based on Archimedes principle, and the density values recorded from 3 independent measurements for each sample were averaged. The microhardness of the composites was measured using an HDX−1000 TMC microhardness tester. The applied load was 50 g and the holding time was 15 s. The recorded microhardness values for each sample were averaged from 10 independent measurements. To obtain compressive mechanical properties of the prepared composites, the specimens with a cross-section of 2 mm × 2 mm and a length of 3 mm were cut from the rolled sheet along the rolling direction. Compression tests were performed on an Instron 3369 universal testing machine at a speed of 1.0 mm/min. The average compression strength of the composites was measured from three samples. The reduced elastic modulus was measured by the Berkovich indenter on a TI950 TRIBO nanoindentation. During the nanoindentation measurement, 20 load-unload circles were used until reaching the maximum load of 80 mN, and the exerted force was subsequently unloaded without holding time. The recorded elastic modulus was obtained from the Oliver−Pharr model [11] and averaged from the measured values of 20 independent tests.

3 Results

3.1 Microstructure of powders and fabricated composites

Figures 2(a−c) show the morphologies of the raw Al powders, Cu powders, and CNTs, respectively. Spherical Al powders (Fig. 2(a)) and irregular Cu powders (Fig. 2(b)) can be observed, which are the typical shapes of powders fabricated by gas atomization and electrolysis. The CNTs present a high aspect ratio and the residual impurities cannot be seen, such as the catalyst particles. Moreover, as shown in the high-resolution TEM image (Fig. 2(d)), the (002) plane of CNTs with the interplanar spacing of 0.34 nm can be detected, demonstrating that the used CNTs have high crystallinity [12]. Figure 2(e) shows the SEM image of the mixed powders of CNTs and Al−Cu alloy powders. It can be seen that the CNTs are singly attached on the surface of Al flakes, and the agglomeration of CNTs is rarely detected, which

confirms that the applied pretreatment process of CNTs and mixing process for mixed powders are capable of realizing the uniform dispersion of CNTs in Al powers.

Figure 3(a) reveals the XRD patterns of the three types of mixed powders. In addition to the Al diffraction peaks, the weak peaks belonging to the AlCu phase can be detected, indicating that the reaction between Al and Cu should be initiated due to the energy input by the ball milling process. Figure 3(b) shows the XRD patterns of the three bulk composites. It can be seen that there are peaks derived from the Al matrix and AlCu phase in all XRD patterns. With increasing the Cu content to 3 and 7 wt.%, the distinct peaks of Al_2Cu can be further found in the XRD patterns, denoting the increased Cu content results in the formation of Al_2Cu precipitates. Moreover, the shift of Al peaks is absent with increasing Cu content, indicating that the Cu was consumed by the Al_2Cu precipitation rather than the formation of Al−Cu solid solution during the composite fabrication processes.

Figure 4 shows the backscattered SEM images of the prepared composites and corresponding EDAX results. It can be seen from Fig. 4 that the particles with bright contrast are uniformly dispersed in the whole Al matrix, and their size and number density increase with increasing the Cu content. According to the EDAX results acquired from the Al−7Cu@CNTs composite, it can be confirmed that the particles consist of Al and Cu elements. Combined with the XRD results (Fig. 3), these newly formed particles with increasing the Cu content can be determined as the Al_2Cu phase.

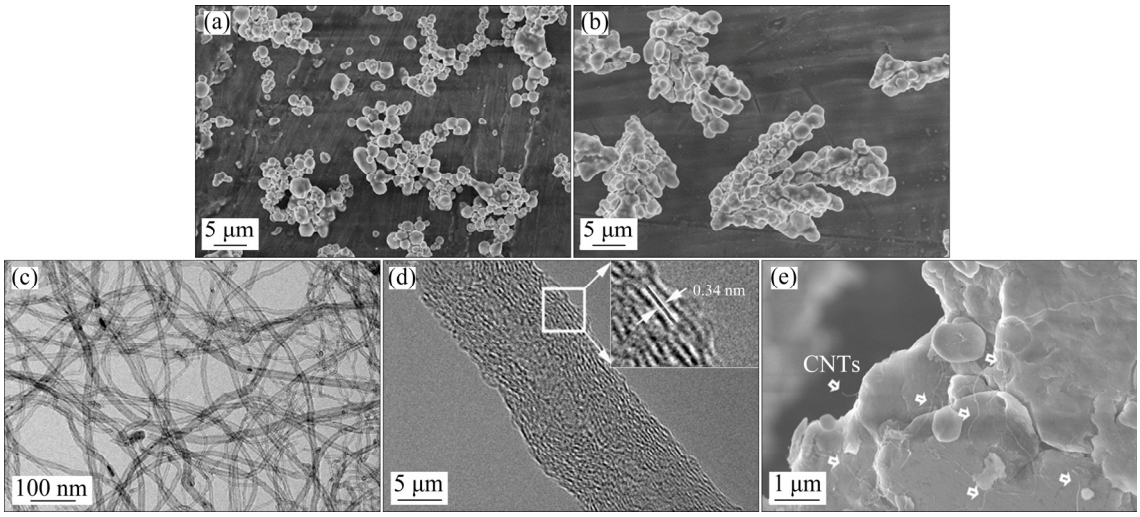

Fig. 2 Microstructures of raw materials and mixed powders: (a, b) SEM images of Al and Cu powders, respectively; (c) Bright-field TEM image of CNTs; (d) High-resolution TEM image of CNTs; (e) SEM image of mixed powders of Al−7wt.%Cu alloy powders and CNTs

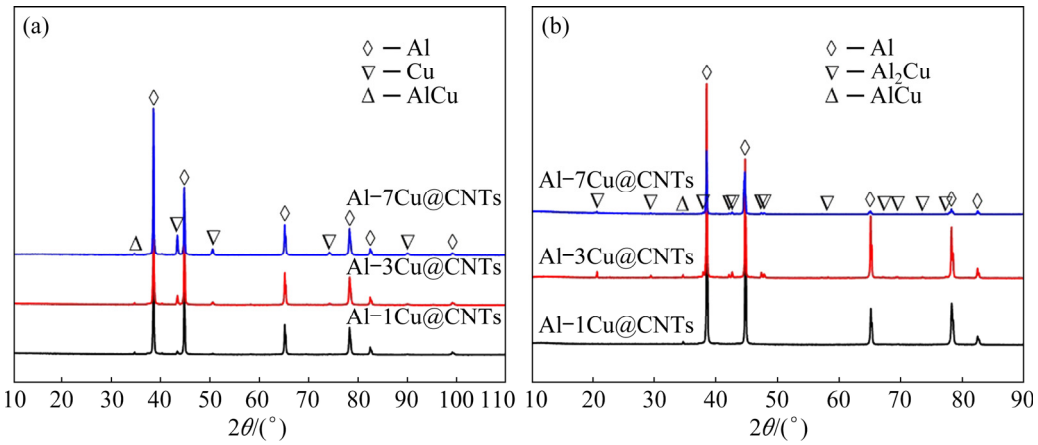

Fig. 3 XRD patterns of three types of mixed powders (a) and fabricated composites (b)

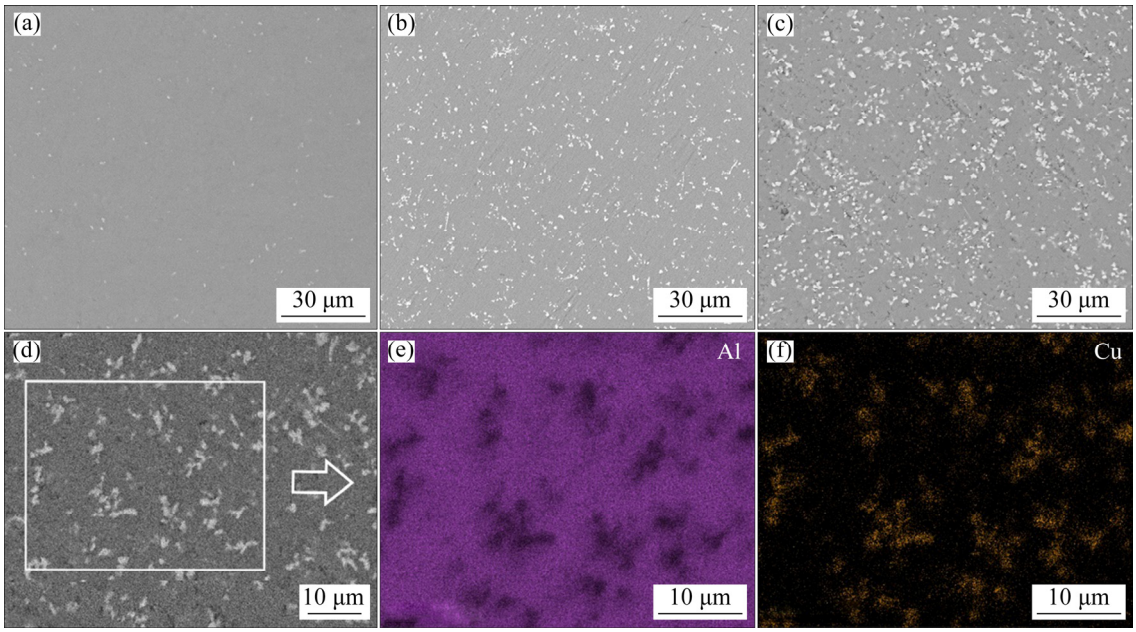

Fig. 4 Microstructures and corresponding EDAX results of fabricated composites: (a, b, c) Backscattered SEM images of Al−1Cu@CNTs, Al−3Cu@CNTs, and Al−7Cu@CNTs, respectively; (d, e, f) Enlarged backscattered SEM image of Al−7Cu@CNTs (d) and obtained EDAX results (e, f)

Figure 5 further presents the statistical analysis results of the size and number density of precipitates in the fabricated composites with different Cu contents. The results show that by increasing the Cu content from 1 wt.% to 7 wt.%, the average particle size of the precipitates increases from 596 to 1282 nm, while the number density of the precipitated phase also increases from 1.42×10^4 to around 6.4×10^4 mm^{-2}. The largely increased particle size and similar number density of precipitates in Al−7Cu@CNTs compared with those in Al−3Cu@CNTs imply that the increase of Cu content from 3 wt.% to 7 wt.% facilitates the growth of Al_2Cu precipitates instead of their new nucleation.

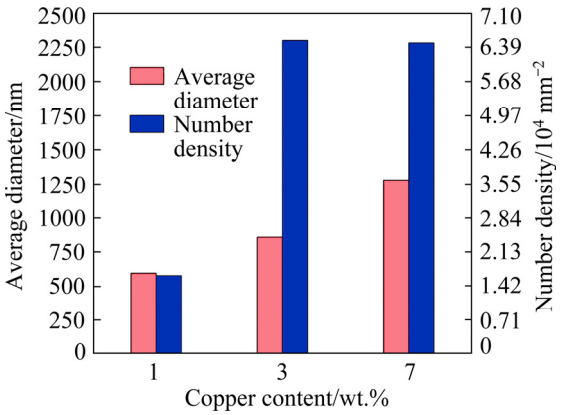

Fig. 5 Statistical results of average diameter and number density of precipitates in fabricated composites based on obtained SEM images

To further reveal the microstructures of the composites with different Cu contents, TEM observation was employed to examine the Al−1Cu@CNTs and Al−7Cu@CNTs composites. Figures 6 and 7 show the typical TEM images acquired from the Al−1Cu@CNTs composite. As

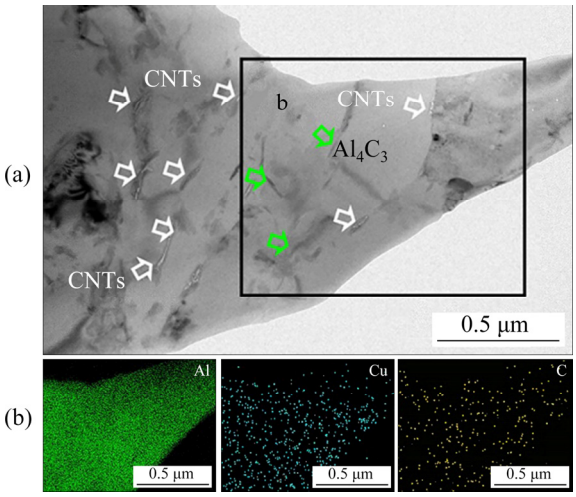

Fig. 6 TEM images of as-fabricated Al−1Cu@CNTs composite: (a) Bright-field TEM image; (b) Elemental mapping results recorded from black rectangle region in (a)

shown in Figs. 6(a), 7(a), and 7(b), a typical homogeneous dispersion of CNTs marked by white hollow arrows in the matrix was realized, while Al_4C_3 with short rod shape and the reaction product of CNTs with the Al matrix, can be occasionally observed. Figure 6(b) shows the elemental mapping results of the rectangle region b in Fig. 6(a), which confirms that most of the Cu element exists in the form of solid solution atoms. The limit formation of the Al−Cu phase can be further justified by the SAED pattern recorded from the red dashed circle region in Fig. 7(b), in which only diffraction spots originated from the Al matrix can be observed. Figures 7(c) and (d) reveal the HRTEM image of the red rectangle region in Fig. 7(b), showing that the CNTs are tightly bonded with the Al matrix, forming a well-bonded Al−CNTs interface, which is essential to exploit the potential strengthening effects of CNTs for Al/CNTs composites.

Figure 8 shows the TEM images of the Al−7Cu@CNTs composite. In comparison to the microstructures of Al−1Cu@CNTs (Figs. 6 and 7), the precipitates and the Al_4C_3 with the length of several hundred nanometers can be commonly observed in the Al−7Cu@CNTs composite (Figs. 8(a−c)). However, it is worth noting that it is hard to detect the CNTs, which implies that with the increase of Cu content, the interfacial reaction between CNTs and Al matrix was significantly promoted, hence causing the complete conversion of CNTs into Al_4C_3. Figures 8(d) and (g) present the elemental point analysis results and HRTEM image from the precipitates, fully confirming that the precipitates are Al_2Cu phases. The SAED pattern (Insert in Fig. 8(b)) and HRTEM images (Figs. 8(e) and (f)) are recorded from the formed Al_4C_3, showing that the in-situ Al_4C_3 with the periodical crystallographic plane and interplanar spacing (0.84 nm) is a highly crystalline single crystal that has a hexagonal structure with lattice parameters of a=0.334 nm and c=2.50 nm [13].

3.2 Mechanical properties of as-prepared composites

The compressive mechanical properties, bulk density, and hardness of the composites are shown in Fig. 9. As can be seen from the compressive properties of the three composites (Fig. 9(a)), the yield strength (YS), ultimate compressive strength (UCS), and failure strain of composites monotonously decrease with increasing the Cu content. The yield strength and ultimate compressive

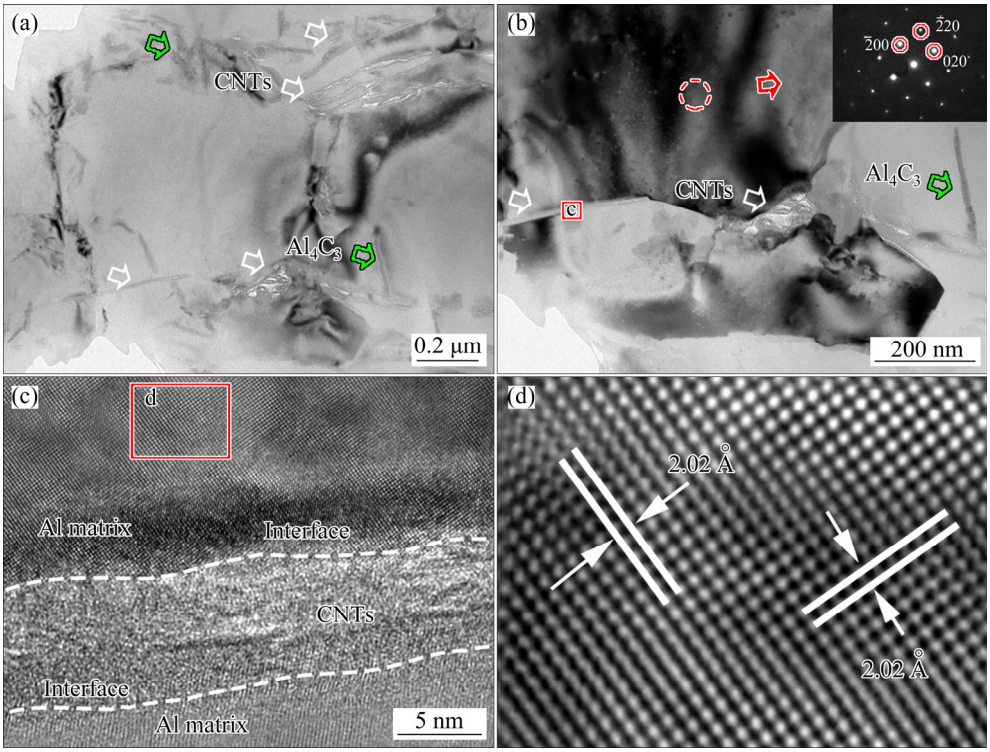

Fig. 7 TEM images of as-fabricated Al−1Cu@CNTs composite: (a, b) Bright-field TEM images (inserted SAED pattern acquired from red dashed circle in (b); (c) HRTEM image of red rectangle region in (b); (d) Magnified image of red rectangle area in (c)

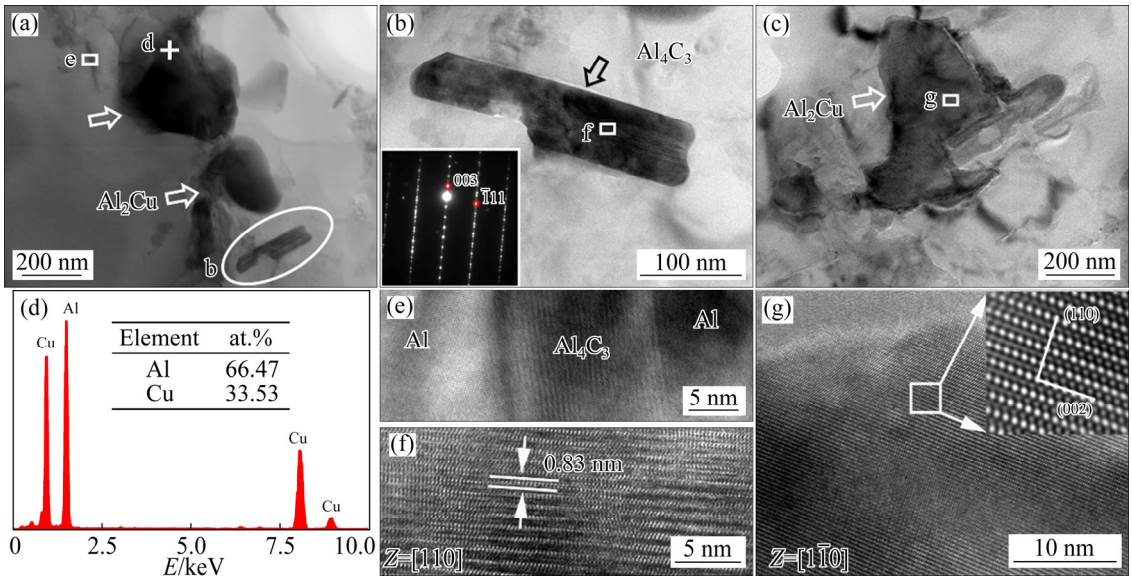

Fig. 8 TEM images of as-fabricated Al−7Cu@CNTs composite: (a) Bright-field TEM image of precipitates and Al_4C_3 rods; (b) Magnified image of white oval region in (a); (c) Enlarged bright-field TEM image of typical precipitate; (d) EDAX point analysis result of precipitate marked by white cross star in (a); (e, f) HRTEM images of white rectangle regions in (a) and (b), respectively; (g) HRTEM image of white rectangle region in (c)

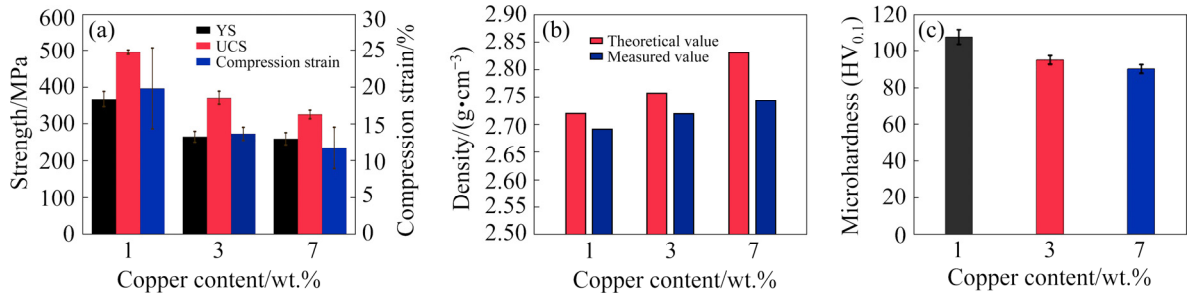

Fig. 9 Variation of mechanical properties of as-prepared composites with Cu content: (a) Ultimate compressive strength, yield strength, and compression strain; (b) Theoretical density and measured bulk density; (c) Microhardness

strength of Al−1Cu@CNTs composite can reach (367.92±21.21) MPa and (495.14±5.68) MPa, respectively, which are much higher than those of Al−7Cu@CNTs composite ((259.96±16.39) MPa and (371.44±18.23) MPa). In addition to the decreased strength, it can be observed that increasing the Cu content from 1 wt.% to 7 wt.% also decreases the ductility of the composites, and the failure strain of the Al−7Cu@CNTs composite is only about 11.8%.

Figure 9(b) exhibits the theoretical density and measured bulk density of the fabricated composites. It can be observed that the material density increases with the increase of Cu content, which is caused by the adoption of Cu element with much higher density than Al element. Although the increased Cu content accelerates the formation of Al_4C_3, and the transformation from CNTs and Al into Al_4C_3 can result in about 6.78% volume expansion by taking the formula mass and density of Al (27 g/mol, 2.7 g/cm^3), CNTs (12 g/mol, 2.1 g/cm^3 [14]) and Al_4C_3 (144 g/mol, 2.36 g/cm^3 [15]), it is believed that the improved density caused by the inclusion of Cu largely surpasses the lowered density induced by the chemical reaction between Al and CNTs. Figure 9(c) shows the measured hardness of the three composites. It can be seen that the hardness decreases from $HV_{0.1}$ (107.7±4.1) to $HV_{0.1}$ (90.1±2.4) with increasing the Cu content from 1 wt.% to 7 wt.%.

Figure 10(a) shows the nanoindentation load−displacement curves consisting of 20 load−unload circles of the prepared composites. It can be seen that the indentation displacement of Al−1Cu@CNTs is significantly smaller than that of Al−3Cu@CNTs and Al−7Cu@CNTs, denoting the

Al−1Cu@CNTs composites possess higher hardness, which is consistent with microhardness results (Fig. 9(c)). Based on the load−displacement curves, the obtained elastic modulus of the three composites is presented in Fig. 10(b). It can be seen that the measured elastic modulus scatters in a wide range for each type of composite, and the average elastic modulus decreases with increasing the Cu content in the composites. The compressive mechanical properties, hardness, density, and elastic modulus of the prepared composites are also listed in Table 1.

4 Discussion

As shown in Figs. 4, 6, 7, and 8, increasing the Cu content promotes the formation of Cu-containing precipitates and intensifies the interfacial reaction between Al matrix and CNTs. According to the Al−Cu phase diagram, five equilibrium phases of Al_2Cu, AlCu, Al_3Cu_4, Al_2Cu_3, and Al_4Cu_9 could be formed in the Al−Cu system [16]. However, higher Cu content only results in the formation of Al_2Cu precipitates in the present study, other Al−Cu phases are absent. In general, the phase formation sequence in a specific alloy system can be determined by the related thermodynamics. In terms of thermodynamics, several models have been proposed to evaluate the precipitation sequence in the binary system, among which the effective heat of formation (EHF) model developed by PRETORIUS et al [17] has been regarded as the most effective method to examine the formation of first precipitations in Al−metal binary system. The EHF is equal to the effective Gibbs free energy change ΔG^0 (ΔG^e) for the formation of phase i, and can be defined as [18]

$$\Delta G_i^e = \Delta G_i^0 \times \frac{C_e}{C_i} \quad (1)$$

where ΔG_i^0 is the Gibbs free energy change (ΔG^0) for the formation of phase i, C_e is the effective concentration of Cu element at the reaction interface, and C_i is the concentration of the Cu element in the formed Al−Cu phase. As presented in Eq. (1), the C_e highly affects the ΔG_i^e, while it is difficult to determine the C_e, which is influenced by many factors such as the lowest eutectic concentration and atomic mobility [18]. Nevertheless, PRETORIUS et al [17] suggested that the C_e can be taken at the lowest eutectic temperature because the highest mobility of the atoms and the most effective mixing at the reaction interface tend to occur with the composition at the lowest eutectic temperature. Based on his proposal, the ΔG_i^e with the Cu compositions of Al_2Cu, AlCu,

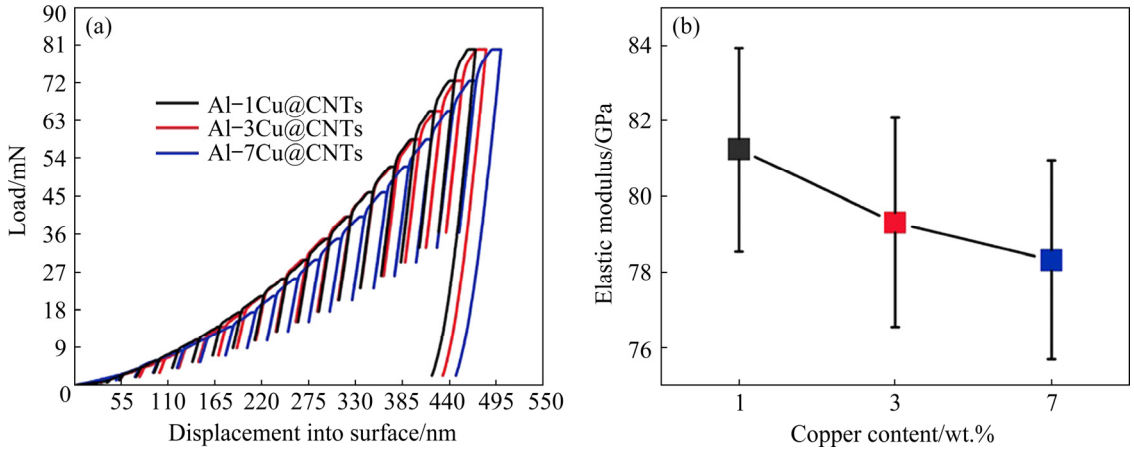

Fig. 10 Nanoindentation results of three composites: (a) Representative load−displacement curves; (b) Elastic modulus obtained from load−displacement curves in (a)

Table 1 Density and mechanical properties of fabricated composites

Composite	YS/ MPa	UCS/ MPa	Compression strain/%	Hardness ($HV_{0.1}$)	Density/ ($g·cm^{-3}$)	Elastic modulus/ GPa
Al−1Cu@CNTs	367.95±12.21	495.14±5.68	19.85±5.50	107.7±4.1	2.693	81.24±2.69
Al−3Cu@CNTs	305.47±8.46	386.21±8.17	13.67±0.88	95.0±2.3	2.720	79.32±2.76
Al−7Cu@CNTs	293.98±10.21	367.58±9.45	11.76±2.80	90.1±2.4	2.745	78.32±2.63

Al_3Cu_4, Al_2Cu_3, and Al_4Cu_9 can be calculated to be −14.21, −19.37, −18.86, −19.01, and −18.58 kJ/mol, respectively. It can be seen that the AlCu formation has the most negative ΔG_i^e, but in the sequence of precipitated phases of the Al−Cu alloy, Al_2Cu is more stable and the long thermal processing time is sufficient to convert AlCu to Al_2Cu, which can explain the fact that increasing Cu content only results in the formation of Al_2Cu in the fabricated composites [19,20].

In addition to the Al_2Cu formation, it can be seen that the size of Al_2Cu increases with increasing the Cu content, which can be attributed to two main possible reasons. On the one hand, the introduced Al−CNTs interface can act as the diffusion path of Cu atoms [21], which facilitates the supply of Cu atoms through the thermodiffusion for the growth of the Al_2Cu phase. On the other hand, a relatively low cooling rate after sintering or hot rolling was adopted for the present fabricated composites, thus the high temperature allows the thermodiffusion of Cu atoms for a long time. Furthermore, the in-situ reaction for Al_2Cu formation is a typical exothermic process [22]. The intensified Al_2Cu formation can provide energy for the reaction of Al and C and reduce the Gibbs free energy change of Al_4C_3 formation accordingly. So, it is believed that the released heat from the Al_2Cu formation should be the main reason for the complete transformation from CNTs to Al_4C_3 in the Al−7Cu@CNTs composite, as shown in Fig. 8.

Based on the microstructure characterization results, it can be seen that the reinforcement characteristics varied with increasing the Cu content. The in-situ formed Al−Cu precipitates and CNTs act as reinforcements in Al−1Cu@-CNTs composite, while the Al−Cu precipitates were substantially coarsened, and CNTs were transformed into Al_4C_3, resulting in different mechanical properties of the other two types of composites. To elucidate the fundamental relationship between the microstructures and mechanical properties, it is necessary to reveal the strength contribution from the related strengthening mechanisms. In general, several strengthening mechanisms have been proposed for the metal matrix composites, mainly including the load transfer strengthening ($\Delta\sigma_{LT}$), Orowan strengthening ($\Delta\sigma_{Orowan}$), coefficient of thermal expansion (CTE) mismatch strengthening ($\Delta\sigma_{CTE}$), and solid solution strengthening ($\Delta\sigma_{SS}$) [23], which strengthening mechanism works depends on the characteristics of the reinforcements. Based on the microstructure characterization results, load transfer strengthening from CNTs ($\Delta\sigma_{LT(CNTs)}$), Orowan strengthening from CNTs ($\Delta\sigma_{Orowan(CNTs)}$) and Al−Cu precipitates ($\Delta\sigma_{Orowan(Al-Cu)}$), coefficient of thermal expansion (CTE) mismatch strengthening from CNTs ($\Delta\sigma_{CTE(CNTs)}$) and Al−Cu precipitates ($\Delta\sigma_{CTE(Al-Cu)}$), and solid solution strengthening of Cu atoms ($\Delta\sigma_{SS(Cu)}$) should work in Al−1Cu@CNTs composite, while Orowan strengthening from Al_4C_3 ($\Delta\sigma_{Orowan(Al_4C_3)}$) and Al−Cu precipitates ($\Delta\sigma_{Orowan(Al-Cu)}$), coefficient of thermal expansion (CTE) mismatch strengthening from Al_4C_3 ($\Delta\sigma_{CTE(Al_4C_3)}$) and Al−Cu precipitates ($\Delta\sigma_{CTE(Al-Cu)}$), and solid solution strengthening of Cu atoms $\Delta\sigma_{SS(Cu)}$ take effects in Al−7Cu@CNTs composite.

As for the Al−1Cu@CNTs composite, the strength increment derives from the load transfer from the Al matrix to CNTs ($\Delta\sigma_{LT(CNTs)}$) can be estimated from the shear-lag theory proposed by KELLY and TYSON [24] as

$$\Delta\sigma_{LT(CNTs)} = V_{CNTs}\tau_m\left[S\cos^2\theta+(1-\frac{4}{3\pi})(1+\frac{1}{S})\sin^2\theta\right] \quad (2)$$

where V_{CNTs} is the volume fraction of CNTs, S is the aspect ratio of CNTs, θ is the angle between CNTs and loading direction, and τ_m is the matrix shear strength. As the CNTs were aligned along with the rolling direction, which is parallel to the loading direction, the θ can be regarded as 0°. The load shear theory is based on the assumption that the reinforcement is well bonded with the metal matrix, which can provide perfect load transfer efficiency across the interface between them. In the present study, the tightly bonded interface between Al matrix and CNTs can be justified by the TEM observation (Fig. 7(c)), so the τ_m can be taken as $\sigma_m/2$ (50 MPa) (σ_m is the yield strength of the Al matrix with value of ~100 MPa [12]). Therefore, it is found that when the V_{CNTs} and S are 0.75 vol.% and 300, respectively, the $\Delta\sigma_{LT(CNTs)}$ can be calculated to be 112.5 MPa.

The enhanced strength from the Orowan strengthening for Al−1Cu@CNTs and Al−7Cu@-CNTs can be theoretically calculated by the

Orowan−Ashby equation [25]:

$$\Delta\sigma_{\text{Orowan}} = \frac{MGb}{2.36\pi}\cdot\ln\left(\frac{\phi}{2b}\right)\cdot\frac{1}{\lambda-\phi} \tag{3}$$

where M is the Taylor factor, taken as 3.06 for fcc polycrystal Al matrix [1], G is the shear modulus (25.4 GPa for Al [26]), b is the amplitude of Burgers vector (0.286 nm for Al [26]), ϕ is the particle diameter, and λ is the interparticle spacing. Assuming that the Al−Cu precipitates are uniformly dispersed in the whole Al matrix and exhibit a simple cubic arrangement, λ can be calculated using the following formula [25]:

$$\lambda = \phi\left(\frac{\pi}{6V_{\text{Al-Cu}}}\right)^{1/3}$$

where $V_{\text{Al-Cu}}$ is the volume fraction of Al−Cu precipitates. Meanwhile, the $V_{\text{Al-Cu}}$ can be estimated from the statistic results given in Fig. 5 using the following equation:

$$V_{\text{Al-Cu}} = 10^{-12}n\pi\left(d/2\right)^2\times100\% \tag{4}$$

where n is the number density (mm^{-2}) and d is the average particle size of the precipitated phase. Hence, the $V_{\text{Al-Cu}}$ for Al−1Cu@CNTs and Al−7Cu@CNTs composites with 1 wt.% and 7 wt.% Cu contents is 0.46% and 8.37%, respectively. Therefore, the $\Delta\sigma_{\text{Orowan(Al-Cu)}}$ for Al−1Cu@CNTs and Al−7Cu@CNTs composites can be calculated to be 9.1 and 21.4 MPa, respectively.

Similar to Al−Cu precipitates, the CNTs in Al−1Cu@CNTs and Al_4C_3 transformed from CNTs in Al−7Cu@CNTs can also block the dislocation movement during the deformation and enhance the material. Owing to the full conversion from 0.75 vol.% CNTs to Al_4C_3, the volume fraction of Al_4C_3 in Al−7Cu@CNTs can be determined as 2.78 vol.% by taking the densities of CNTs and Al_4C_3 as 2.1 and 2.36 g/cm^3, respectively. For the Orowan strengthening mechanism of Al_4C_3 and CNTs, it also obeys the rule illustrated in Eq. (3), while the particle diameter ϕ should be replaced with the equivalent diameter (ϕ_{eq}) for rod-shaped reinforcement, which is given by

$$\phi_{\text{eq}} = \sqrt[3]{\frac{3D^2L}{2}} \tag{5}$$

where D and L are the diameter and length of Al_4C_3 or CNTs, respectively. The D and L of Al_4C_3 can be directly measured as 68 and 319 nm, respectively through the TEM observation. Thus, $\Delta\sigma_{\text{Orowan(CNTs)}}$ in Al−1Cu@CNTs and the $\Delta\sigma_{\text{Orowan}(Al_4C_3)}$ in Al−7Cu@CNTs can be calculated as 111.5 and 75.1 MPa, respectively.

During the composite fabrication process, the mismatch of thermal expansion coefficient between the reinforcements ($2.1\times10^{-5}\,\text{K}^{-1}$ for CNTs [27], $1.7\times10^{-5}\,\text{K}^{-1}$ for Al_2Cu [28], and $0.5\times10^{-5}\,\text{K}^{-1}$ for Al_4C_3 [29]) and the Al matrix ($2.3\times10^{-5}\,\text{K}^{-1}$ [30]) generates dislocations in the Al matrix. The increased dislocation density within the matrix can increase the strength of the fabricated composites. The enhanced strength from thermal mismatch ($\Delta\sigma_{\text{CTE}}$) can be calculated using the following equation [23]:

$$\Delta\sigma_{\text{CTE}} = kGb\sqrt{\rho} \tag{6}$$

where k is a constant (~1.25 [31]), and ρ is the enhanced dislocation density, which can be estimated as follows [23]:

$$\rho = 12\frac{\Delta\alpha\Delta TV_{\text{R}}}{b\phi(1-V_{\text{R}})} \tag{7}$$

where $\Delta\alpha$ is the difference in thermal expansion coefficients between the Al matrix and the reinforcements, ΔT is the difference between the temperature in the hot rolling process (723 K) and the temperature during mechanical properties testing (298 K), and V_{R} is the volume fraction of each type of reinforcement. In the present case, the ϕ for rod-shaped CNTs and Al_4C_3 can be replaced with ϕ_{eq} (35.6 nm for CNTs and 130.3 nm for Al_4C_3). $\Delta\sigma_{\text{CTE(CNTs)}}$ and $\Delta\sigma_{\text{CTE(Al-Cu)}}$ in Al−1Cu@CNTs, and $\Delta\sigma_{\text{CTE}(Al_4C_3)}$ and $\Delta\sigma_{\text{CTE(Al-Cu)}}$ in Al−7Cu@CNTs can be calculated to be 25.2, 8.3 MPa, and 76.2, 25.3 MPa, respectively.

For the Al−Cu system, Cu can dissolve into the Al matrix before precipitation, forming Al−Cu solid solution. It is noted that the solubility limit of Cu in Al is ~0.15 at.% at the processing temperature (723 K) [32]. The solid solution strengthening mechanism from Cu atoms can be determined as follows [33]:

$$\Delta\sigma_{\text{ss(Cu)}} = M\frac{G\varepsilon_{\text{ss}}^{3/2}\sqrt{c}}{700} \tag{8}$$

$$\varepsilon_{\text{ss}} = \left|\varepsilon_G' - \beta\varepsilon_b\right| \tag{8a}$$

$$\varepsilon'_G = \frac{\varepsilon_G}{1+|\varepsilon_G|/2} \tag{8b}$$

$$\varepsilon_G = \frac{1}{G}\cdot\frac{\mathrm{d}G}{\mathrm{d}c} \tag{8c}$$

$$\varepsilon_b = \frac{1}{a}\cdot\frac{\mathrm{d}a}{\mathrm{d}c} \tag{8d}$$

where c is the atomic concentration of a solute (0.0015), β is 3 [33], a is the lattice parameter of the Al matrix, 0.404 nm, and ε_{SS} is misfit parameter. Combined with the shear modulus and lattice parameter of Cu (39 GPa and 0.3597 nm), ε_G and ε_b are 0.535 and −0.109, respectively. Finally, $\Delta\sigma_{SS(Cu)}$ can be calculated as 2.7 MPa in Al−1Cu@CNTs and Al−7Cu@CNTs composites.

Assuming that the yield strength of the fabricated composite equals the sum of matrix yield strength and the contribution from the related strengthening mechanisms [23,25,33,34], that is, $\sigma_{YS(Al-1Cu@CNTs)} = \sigma_M + \Delta\sigma_{LT(CNTs)} + \Delta\sigma_{Orowan(CNTs)} + \Delta\sigma_{Orowan(Al-Cu)} + \Delta\sigma_{CTE(CNTs)} + \Delta\sigma_{CTE(Al-Cu)} + \Delta\sigma_{SS(Cu)}$, $\Delta\sigma_{YS(Al-7Cu@CNTs)} = \Delta\sigma_M + \Delta\sigma_{Orowan(Al_4C_3)} + \Delta\sigma_{Orowan(Al-Cu)} + \Delta\sigma_{CTE(Al_4C_3)} + \Delta\sigma_{CTE(Al-Cu)} + \Delta\sigma_{SS(Cu)}$, the theoretically calculated YS of Al−1Cu@CNTs and Al−7Cu@CNTs is 369.3 and 300.7 MPa, respectively, which agree well with the measured YS of the two types of composites. In addition, it is worth noting that the load transfer strengthening and Orowan strengthening from CNTs account for a relatively large proportion (about 83%) in the total yield strength enhancement, denoting that they are the main strengthening mechanisms for the high strength of Al−1Cu@CNTs composite. Whereas, the Orowan strengthening and thermal mismatch strengthening from in-situ formed Al_4C_3 play a major role in enhancing the Al−7Cu@CNTs composite, and the strength contribution from Al_4C_3 is much smaller than that from CNTs in Al−1Cu@CNTs composite.

In short, based on the experimental examination and theoretical calculation results, it can be concluded that increasing the Cu content in Al/CNTs composite results in the strength deterioration, which can be reasonably explained by the changed strengthening mechanisms caused by the consumption of CNTs by the in-situ chemical reaction between Al matrix and CNTs. So, to develop the CNTs reinforced Al−Cu alloy matrix composite with high mechanical properties, it is necessary to protect the CNTs from transforming into Al_4C_3 using proper tactics in the future, such as alloy composition optimization or pre-coating Cu on the surface of CNTs.

5 Conclusions

(1) The Cu content significantly affects the microstructure of the prepared composites, as evidenced by the simultaneous increase in both the size and content of Al−Cu precipitates in the prepared composites with the increase in Cu content. In addition, higher Cu content also intensifies the interfacial reaction between CNTs and Al matrix, causing the conversion of CNTs to Al_4C_3.

(2) The compressive strength, elastic modulus, and microhardness of the prepared composites monotonically decrease with increasing the Cu content; the Al−1Cu@CNTs composite exhibits the best mechanical properties.

(3) The deterioration of the mechanical properties of the composites with increasing Cu content is mainly due to the changed strengthening mechanisms related to the transformation of CNTs into Al_4C_3. In Al−1Cu@CNTs composite, load transfer strengthening and Orowan strengthening from CNTs are the dominant strengthening mechanisms, while Orowan strengthening and thermal mismatch strengthening are the main strengthening mechanisms for Al−7Cu@CNTs composite from CNTs.

Acknowledgments

The financial supports from the National Natural Science Foundation of China (Nos. 52004101 and 52071269), the Chinese Postdoctoral Science Foundation (No. 2020T130246), the Fund of the State Key Laboratory of Solidification Processing in NWPU, China (No. SKLSP202121), the Guangdong Basic and Applied Basic Research Foundation, China (No. 2020A1515110621), and the Fundamental Research Funds for the Central Universities, China (No. 11620345) are appreciated.

References

[1] ZHOU Wei-wei, ZHOU Zhen-xing, KUBOTA K, ONO H, NOMURA N, KAWASAKI A. Design of high-performance Al_4C_3/Al matrix composites for electric conductor [J]. Materials Science and Engineering A, 2020, 798: 140331.

[2] YASHPAL C S, JAWALKAR C S, VERMA A S, SURI N M.

Fabrication of aluminium metal matrix composites with particulate reinforcement: A review [J]. Materials Today: Proceedings, 2017, 4(2): 2927−2936.

[3] TOOZANDEHJANI M, OSTOVAN F, JAMALUDIN K R, AMRIN A, MATORI K A, SHAFIEI E. Process−microstructure−properties relationship in Al−CNTs−Al_2O_3 nanocomposites manufactured by hybrid powder metallurgy and microwave sintering process [J]. Transactions of Nonferrous Metals Society of China, 2020, 30(9): 2339−2354.

[4] JAGANNATHAM M, CHANDRAN P, SANKARAN S, HARIDOSS P, NAYAN N, BAKSHI S R. Tensile properties of carbon nanotubes reinforced aluminum matrix composites: A review [J]. Carbon, 2020, 160: 14−44.

[5] AGARWAL A, LAHIRI D, BAKSHI S R. Carbon nanotubes: Reinforced metal matrix composites [M]. New York: CRC Press, 2018.

[6] MA Kai, LIU Zhen-yu, LIU Kun, CHEN X G, XIAO Bo-lü, MA Zong-yi. Structure optimization for improving the strength and ductility of heterogeneous carbon nanotube/Al−Cu−Mg composites [J]. Carbon, 2021, 178: 190−201.

[7] LI Chun-hong, QIU Ri-sheng, LUAN Bai-feng, HE Wei-jun, LI Zhi-qiang. Hot deformation and processing maps of as-sintered CNT/Al−Cu composites fabricated by flake powder metallurgy [J]. Transactions of Nonferrous Metals Society of China, 2018, 28(9): 1695−1704.

[8] SHIN S E, BAE D H. Deformation behavior of aluminum alloy matrix composites reinforced with few-layer graphene [J]. Composites Part A: Applied Science and Manufacturing, 2015, 78: 42−47.

[9] GUO Bai-song, ZHANG Xin-ming, CEN Xi, CHEN Biao, WANG Xin-hua, SONG Min, NI Song, YI Jian-hong, SHEN Tao, DU Yong. Enhanced mechanical properties of aluminum based composites reinforced by chemically oxidized carbon nanotubes [J]. Carbon, 2018, 139: 459−471.

[10] GUO Bai-song, LUO Si-wei, WU Yue, SONG Min, CHEN Biao, YU Zhen-tao, LI Wei. Regulating the interfacial reaction between carbon nanotubes and aluminum via copper nano decoration [J]. Materials Science and Engineering A, 2021, 820: 141576.

[11] KANG Ji-jun, BECKER A A, WEN Wu, SUN Wei. Extracting elastic-plastic properties from experimental loading−unloading indentation curves using different optimization techniques [J]. International Journal of Mechanical Sciences, 2018, 144: 102−109.

[12] GUO Bai-song, CHEN Yi-qiang, WANG Zhang-wei, YI Jian-hong, NI Song, DU Yong, LI Wei, SONG Min. Enhancement of strength and ductility by interfacial nano-decoration in carbon nanotube/aluminum matrix composites [J]. Carbon, 2020, 159: 201−212.

[13] ZHOU Wei-wei, DONG Ming-qi, ZHOU Zheng-xin, SUN Xiao-hao, KIKUCHI K, NOMURA N, KAWASAKI A. In situ formation of uniformly dispersed Al_4C_3 nanorods during additive manufacturing of graphene oxide/Al mixed powders [J]. Carbon, 2019, 141: 67−75.

[14] BAKSHI S R, AGARWAL A. An analysis of the factors affecting strengthening in carbon nanotube reinforced aluminum composites [J]. Carbon, 2011, 49: 533−544.

[15] DU Jun, SHI Yu-tong, LI Wen-fang. Assessment of solidification characteristics of carbon-inoculated Mg−3%Al melt by thermal analysis [J]. Transactions of Nonferrous Metals Society of China, 2018, 28(4): 812−818.

[16] ZOBAC O, KROUPA A, ZEMANOVA A, RICHTER K W. Experimental description of the Al−Cu binary phase diagram [J]. Metallurgical and Materials Transactions A, 2019, 50(8): 3805−3815.

[17] PRETORIUS R, MARAIS T, THERON C. Thin film compound phase formation sequence: An effective heat of formation model [J]. Materials Science Reports, 1993, 10(1/2): 1−83.

[18] PRETORIUS R, VREDENBERG A M, SARIS F W, REUS R. Prediction of phase formation sequence and phase stability in binary metal−aluminum thin-film systems using the effective heat of formation rule [J]. Journal of Applied Physics, 1991, 70(7): 3636−3646.

[19] ZHOU Dong-shuai, QIU Feng, JIANG Qi-chuan. Simultaneously increasing the strength and ductility of nano-sized TiN particle reinforced Al–Cu matrix composites [J]. Materials Science and Engineering A, 2014, 596: 98−102.

[20] TIAN Wei-si, ZHAO Qing-long, ZHANG Qing-quan, QIU Feng, JIANG Qi-chuan. Enhanced strength and ductility at room and elevated temperatures of Al−Cu alloy matrix composites reinforced with bimodal-sized TiC_p compared with monomodal-sized TiC_p [J]. Materials Science and Engineering A, 2018, 724: 368−375.

[21] GONG Tai-min, YAO Ping-ping, XIONG Xiang, ZHOU Hai-bin, ZHANG Zhong-yi, XIAO Ye-long, ZHAO Lin, DENG Min-wen. Microstructure and tribological behavior of interfaces in Cu−SiO_2 and Cu−Cr metal matrix composites [J]. Journal of Alloys and Compounds, 2019, 786: 975−985.

[22] TIAN Jin-zhong, ZHAO Yu-hong, HOU Hua, HAN Pei-de. First-principles investigation of the structural, mechanical and thermodynamic properties of Al_2Cu phase under various pressure and temperature conditions [J]. Solid State Communications, 2017, 268: 44−50.

[23] PARK J G, KEUM D H, LEE Y H. Strengthening mechanisms in carbon nanotube-reinforced aluminum composites [J]. Carbon, 2015, 95: 690−698.

[24] KELLY A, TYSON A W. Tensile properties of fibre-reinforced metals: Copper/tungsten and copper/molybdenum [J]. Journal of the Mechanics and Physics of Solids, 1965, 13(6): 329−350.

[25] CHEN Biao, SHEN Jiang-hua, YE Xiao-xin, JIA Lei, LI Shu-feng, UMEDA J, TAKAHASHI M, KONDOH K. Length effect of carbon nanotubes on the strengthening mechanisms in metal matrix composites [J]. Acta Materialia, 2017, 140: 317−325.

[26] GUO Bai-song, NI Song, YI Jian-hong, SHEN Ru-juan, TANG Zhong-hua, DU Yong, SONG Min. Microstructures and mechanical properties of carbon nanotubes reinforced pure aluminum composites synthesized by spark plasma sintering and hot rolling [J]. Materials Science and Engineering A, 2017, 698: 282−288.

[27] SHIRASU K, NAKAMURA A, YAMAMOTO G, OGASAWARA T, SHIMAMURA Y, INOUE Y, HASHIDA T. Potential use of CNTs for production of zero thermal

expansion coefficient composite materials: An experimental evaluation of axial thermal expansion coefficient of CNTs using a combination of thermal expansion and uniaxial tensile tests [J]. Composites Part A: Applied Science and Manufacturing, 2017, 95: 152−160.

[28] DINAHARAN I, BALAKRISHNAN M, SELVAM J D R, AKINLABI E T. Microstructural characterization and tensile behavior of friction stir processed AA6061/Al_2Cu cast aluminum matrix composites [J]. Journal of Alloys and Compounds, 2019, 781: 270−279.

[29] GUO Bai-song, CHEN Biao, ZHANG Xin-ming, CEN Xi, WANG Xin-hua, SONG Min, NI Song, YI Jian-hong, SHEN Tao, DU Yong. Exploring the size effects of Al_4C_3 on the mechanical properties and thermal behaviors of Al based composites reinforced by SiC and carbon nanotubes [J]. Carbon, 2018, 135: 224−235.

[30] NYANOR P, EL-KADY O, YEHIA H M, HAMADA A S, NAKAMURA K, HASSAN M A. Effect of carbon nanotube (CNT) content on the hardness, wear resistance and thermal expansion of in-situ reduced graphene oxide (rGO)-reinforced aluminum matrix composites [J]. Metals and Materials International, 2021, 27(5): 1315−1326.

[31] HANSEN N. The effect of grain size and strain on the tensile flow stress of aluminium at room temperature [J]. Acta Metallurgica, 1977, 25(8): 863−869.

[32] WEI Yan-ni, LI Jing-long, XIONG Jian-tao, ZHANG Fu-sheng. Investigation of interdiffusion and intermetallic compounds in Al−Cu joint produced by continuous drive friction welding [J]. Engineering Science and Technology, an International Journal, 2016, 19(1): 90−95.

[33] WEN Hai-ming, TOPPING T D, ISHEIM D, SEIDMAN D N, LAVERNIA E J. Strengthening mechanisms in a high-strength bulk nanostructured Cu–Zn–Al alloy processed via cryomilling and spark plasma sintering [J]. Acta Materialia, 2013, 61(8): 2769−2782.

[34] TANG Fei, ANDERSON I E, GNAUPEL-HEROLD T, PRASK H. Pure Al matrix composites produced by vacuum hot pressing: Tensile properties and strengthening mechanisms [J]. Materials Science and Engineering A, 2004, 383(2): 362−373.

Cu 含量对 CNTs/Al−Cu 复合材料显微组织和压缩力学性能的影响

罗思伟[1]，吴 悦[1]，陈 彪[2]，宋 昡[3]，易健宏[4]，郭柏松[1,5]，王启伟[1]，杨 勇[5]，李 卫[1]，于振涛[1]

1. 暨南大学 先进耐磨蚀及功能材料研究院，广州 510632；
2. 西北工业大学 凝固技术国家重点实验室，西安 710072；
3. 中南大学 粉末冶金国家重点实验室，长沙 410083；
4. 昆明理工大学 材料科学与工程学院，昆明 650093；
5. 香港城市大学 材料科学及工程系，香港 999077

摘 要：通过热压烧结和热轧制备碳纳米管(CNTs)增强的 Al−Cu 基复合材料，系统研究 Cu 含量对 Al 与 CNTs 的界面反应、含 Cu 沉淀物的析出行为及相应复合材料力学性能的影响。研究表明，提高 Cu 含量不仅能使复合材料制备过程中含 Cu 析出相的数量和尺寸增加，而且能促进 CNTs 与 Al 基体之间的界面反应，加剧 CNTs 转化为 Al_4C_3。由于含有 1% Cu(质量分数)的复合材料保持 CNTs 的原始结构，因此，它在所有复合材料中具有最高的强度、弹性模量和硬度。此外，增加 Cu 含量还能改变影响复合材料强度的主要强化机制。

关键词：铝基复合材料；Al−Cu 析出相；碳纳米管；界面反应；强化机制

(Edited by Wei-ping CHEN)